Research Square

Preprints are preliminary reports that have not undergone peer review.
They should not be considered conclusive, used to inform clinical practice,
or referenced by the media as validated information.

Strategic retirement enhances electric vehicle battery circularity

Hanyu Bai
University of Michigan–Ann Arbor
Yichen Liang
National University of Singapore
Qiuhao Hu
bhu@farasis.com

Farasis Energy (United States)
Yao Ren
Farasis Energy (United States)
Qi Jiao
Farasis Energy (United States)
Yufei Yuan
National University of Singapore
Weiran Jiang
wjiang@farasis.com

Farasis Energy (United States)
Ziyou Song
ziyou@umich.edu

University of Michigan–Ann Arbor

Research Article

Keywords:

Posted Date: September 7th, 2026

DOI: https://doi.org/10.21203/rs.3.rs-10923974/v1

License: This work is licensed under a Creative Commons Attribution 4.0 International License.
Read Full License

Additional Declarations: The authors declare no competing interests.

Strategic retirement enhances electric vehicle battery circularity

Hanyu Bai[1†], Yichen Liang[2†], Qiuhao Hu[3*], Yao Ren[3], Qi Jiao[3], Yufei Yuan[2], Jiawei Zhang[1], Weiran Jiang[3*], Ziyou Song[1*]

[1]Department of Electrical Engineering and Computer Science, University of Michigan, Ann Arbor, MI, USA.
[2]Department of Mechanical Engineering, National University of Singapore, Singapore, Singapore.
[3] Farasis Energy USA, Inc., Hayward, CA, USA.

[†]These authors contributed equally to this work.

Abstract

Reusing retired electric vehicle (EV) batteries offers an immediate pathway to meet rising energy-storage demand, but current retirement practices limit their adoption. Here, we systematically evaluate more than 10,000 EV battery lifecycle pathways from in-vehicle operation to second-life applications, quantifying how retirement decisions affect reuse value. We find that strategic retirement can enable effective reuse, where retiring EV batteries 1-2 years earlier on average can shift 40-50% of them from being unreusable to reusable, unlocking terawatt-hour-scale energy storage capacity and yielding substantial environmental benefits. To enable scalable implementation of strategic retirement, we propose a dynamic trade-in solution, supported by a retirement indicator to guide real-time decisions and a general framework applicable across battery designs for strategy development. This work demonstrates that a minor change in current retirement practices can shift used EV batteries from depreciating assets into value-generating resources with enhanced circularity, highlighting the importance of strategic energy planning in addressing sustainable challenges.

As the cornerstone of the global transition to electric mobility[1,2], lithium-ion batteries are projected to exceed 3 terawatt-hour (TWh) worldwide by 2030[3–5]. However, existing end-of-life (EOL) pathways (i.e., reusing and recycling) fall short of efficient circularity[6–8]. Despite advances in recycling technologies, there are concerns over low collection rates[9], high costs[10], and regional disparities[6,11] that make recycling alone insufficient to overcome the growing challenges of raw-material scarcity and constrained battery manufacturing capacity[10–12]. Reusing electric-vehicle (EV) batteries offers an immediate and scalable pathway[13–15] to relieve pressures on mineral supply[16,17], manufacturing[18,19], and cost[20], while extending battery service lifetimes to support growing energy-storage demands in power systems[12]. Despite these potential benefits, considerable debate remains over whether second-life use of retired EV batteries is worthwhile.

The reuse value of retired batteries depends on their lifetime and benefits in second-life applications. It varies across batteries with different usage histories and retirement timing in EVs. Compared with continued operation in EVs, intuitively, batteries reused in low-demand power systems should experience slower degradation and longer service lifetimes[21,22]. However, the lack of systematic understanding of reuse potential across different EV batteries[23] and accessible evaluation tools, raises concerns that improper reuse could accelerate degradation (Fig. 1a). More critically, in the absence of clear retirement guidance, EV batteries are often retired only after owners can no longer tolerate range loss from capacity fade—a practice we define as "passive retirement," driven by high replacement costs and limited returns from direct recycling. Such extended in-vehicle use exposes batteries to more severe aging, thereby increasing perceived risks of reuse. These concerns have long fueled the misconception that battery reuse is not a viable solution despite the lack of direct evidence. Consequently, EV batteries retired under current practices are not being reused effectively.

With a large wave of EV battery retirements expected over the coming decades[24] and extended responsibility regulations in the European Union, the United States, and China requiring battery original equipment manufacturers (OEMs) to manage retired batteries, there is an urgent need to develop timely strategies that guide battery retirement for effective reuse. Strategy design requires predictive lifecycle analysis to identify optimal decision pathways that maximize systems' lifecycle values in order to shape a sustainable future before user behaviors, industrial practices, and policies become entrenched[25–29]. However, it has only received limited attention across different fields, such as Earth system science[27,28], biology[30], and energy systems research[26,31]. Existing approaches rely on expert judgment, such as Delphi surveys[32], or build on empirical data and computational tools, yet they are not applicable to EV batteries due to key technical barriers.

Specifically, to assess how different retirement decisions impact EV battery lifecycle values from first to second life, we first need to address how driving behavior and climate jointly shape heterogeneous battery degradation, which remains an open question due to inaccessible real-world operating data[33]. This results in unknown battery health conditions at retirement, and estimating their lifetime in second-life applications is challenging due to the path-dependent nature of battery degradation trajectories. For example, batteries with similar state-of-health (SOH) values can exhibit different lifetimes under the same second-life application, as differences in prior operating history may lead to distinct degradation modes. Capturing the path-dependent degradation requires lifecycle experiments across driving behavior, climate, retirement timing, and reuse scenarios. However, the combinatorial growth in experimental conditions arising from the high-dimensional design space (Fig. 1d) makes experimental exploration prohibitively expensive and impractical to scale for battery systems[34,35]. Physics-based and data-driven models can reduce the experimental costs of such analyses[35,36]; however, most existing models are developed for fresh batteries and lifecycle datasets spanning in-vehicle operation to second-life application are still missing. Therefore, when EV batteries should be retired and how to reuse these batteries remain open questions.

To address these questions, we first draw evidence from commercial EV battery degradation experiments to understand how representative driving behaviors and climates ultimately affect EV battery health conditions at retirement. Then, we systematically evaluate 10,935 potential EV battery lifecycle pathways to assess the impact of retirement timing on EV battery reuse values, based on combinations of diverse driving behaviors, seasonal climates, retirement mileages, and 56 second-life applications across 16 countries (Fig. 2b). To bypass the need for extensive experiments, we propose the physics-augmented learning (PAL, Fig. 1e) framework, a scalable approach validated with our unique dataset for predictive lifecycle analysis. Specifically, this framework exploits existing design-validation data for EV batteries to model retired batteries and estimate their lifetimes for second-life applications (Fig. 1d). It offers three key advantages: (1) capturing path-dependent degradation from the first-life to the second-life, neglecting which can introduce errors in reuse value evaluation; (2) assessing how human behaviors affect battery lifecycle performance from technical, economic, and environmental perspectives; and (3) supporting broad application across commercial batteries with design-validation data.

We find that a minor change in current retirement practices can enable effective reuse, benefiting both EV owners and industrial leaders by turning EV batteries from depreciating assets into value-generating resources. We demonstrate that strategic retirement of EV batteries 1–2 years earlier on average than the current practice can shift 40–50% of them from being unreusable to reusable, equivalent to around 1.5 TWh of storage capacity from more than 100 million retired battery units[4]. This also helps reduce raw material consumption per kilowatt-hour of stored electricity by 27–74% and extend battery service life by 4–5 years. To motivate public participation in strategic retirement, we propose a proactive trade-in plan as a mutually beneficial solution (Fig. 1c). For practical implementation of our solution, we identify a general retirement indicator for the battery management system (BMS) to deliver real-time, dynamic trade-in recommendations to EV owners. Together, these efforts help advance battery circularity and highlight the importance of strategy planning for more sustainable energy and transportation systems.

Health conditions of retired EV batteries

To assess how driving behaviour and climate influence long-term battery degradation, we analysed cycle-life tests of commercial EV batteries under representative driving profiles from urban, aggressive and taxi drivers and seasonal climate conditions, including hot, cold and reference environments (see Methods). Each test corresponds to more than 240,000 km of driving.

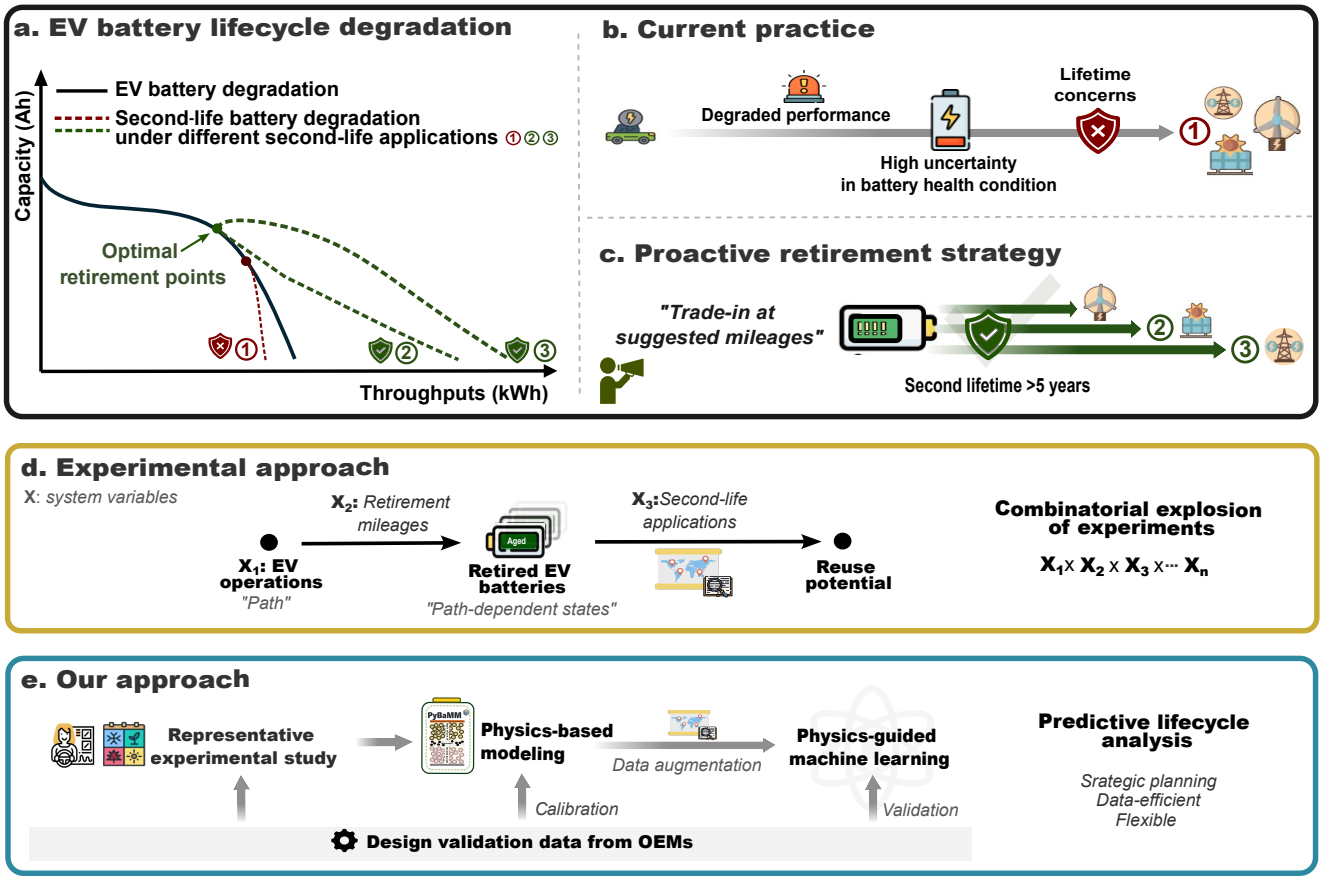


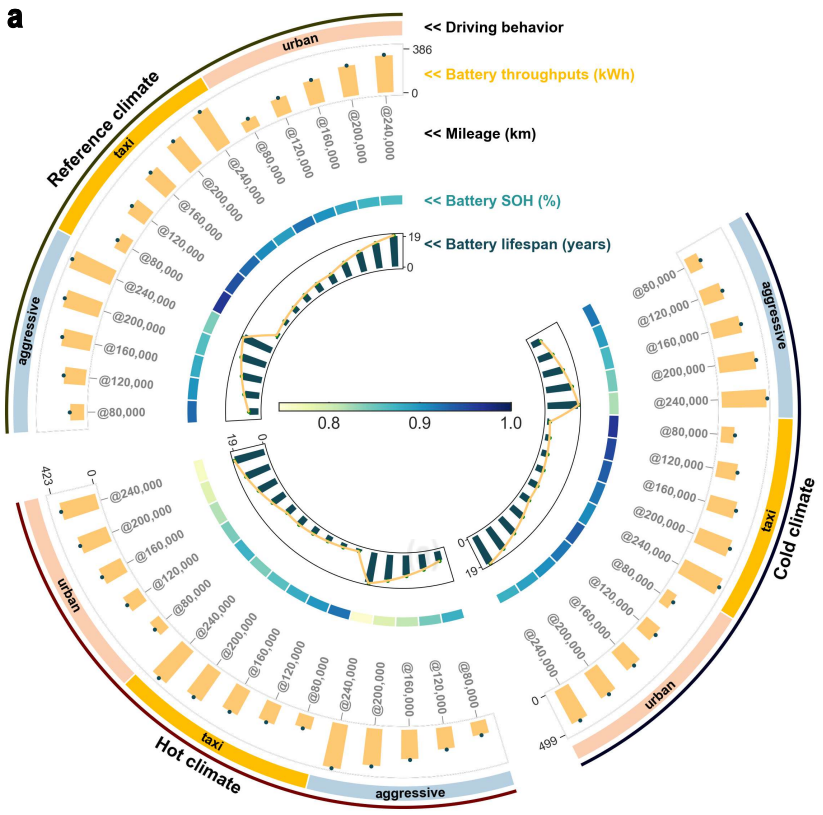
Fig. 1: *Comparison between strategic retirement and current retirement practice on the EV lifecycle value and between the conventional experimental approach and the proposed PAL framework.* ***(a)*** *Lifecycle degradation of batteries, from first-life usage in EVs to second-life usage in power systems.* ***(b)*** *Current passive retirement practice results in retired EV batteries having little reuse potential.* ***(c)*** *Proactive retirement strategies proposed in this study can help extend the lifecycle value of EV batteries by effective reuse.* ***(d)*** *Experimental approaches applied to path-dependent systems that involve sequential behaviors are unscalable because of the combinatorial explosion problem, where the total number of required experiments equals the product of all possibilities.* ***(e)*** *The illustration of the structural design of the PAL framework.*

Different driving behaviors result in different cycling and calendar aging over time. Comparing battery aging at the reference climate (Fig. 2a), EV batteries used by aggressive drivers have the lowest SOH. Their batteries experienced more cycling aging during daily operations due to high average discharge currents (Supplementary Table 5), depths of discharge (Supplementary Fig. 2), and frequent fast-charging events (Supplementary Table 5). These operating features can induce lithium plating and accelerate active material loss driven by particle cracking[37]. Batteries used by taxi drivers have the highest SOH, as they experience less calendar aging due to their near-continuous daily operation.

Climatic factors further diversify battery aging (Fig. 2a). Seasonal temperature variations can accelerate battery aging through Arrhenius-type temperature-dependent aging mechanisms. For example, calendar aging driven by SEI growth accelerates as temperatures rise[38], resulting in capacity loss increasing from 2.16% to 7.4% for taxi drivers from cold land and hot land. Moreover, air conditioners require up to 30% additional energy for heating and cooling[39], resulting in higher energy consumption per mile and greater cycling aging at the same mileage (Extended Data Table 3). In short, different in-vehicle operations lead to heterogeneous battery health over time, resulting in varying reuse potential.

Impact of retirement mileage on reuse potential

To quantify the effect of retirement mileage on battery reuse, we developed the PAL framework, which evaluates reuse value across alternative lifecycle pathways (Fig. 1e). For batteries tested under nine representative real-world operating conditions (Fig. 2a) and assumed to be retired at five different mileages, PAL estimates the remaining useful life (RUL) across 56 second-life applications, with up to eight battery sizes considered for each application



Location	Category	Number of profiles
Australia	RES	1
Cameroon	RES	3
China	ARB	2
	PS	1
Croatian	ARB	1
Denmark	RES	1
Finland	FR	1
France	FR	1
	RES, MG	2
Singapore	FCS	2
	VVC	1
South Korea	PS, FCS	1
Sweden	PS	1
Switzerland	FR	2
	FR, PS	1
Thailand	MG	1
	RES	1
United Arab Emirates	RES, MG	4
United Kingdom	ARB	1
United States of America	ARB	3
	PS	9
	RES	5
Vietnam	RES	1
Unknown	FR	4
	MG	1
	PS	1
	RES	2
	RES, MG	1
	VVC +PS	1

Fig. 2: *Representative experimental study results of 9 combinations of EV battery operations (Extended Data Table 2) and a summary of second-life scenarios from the literature.* ***(a)*** *Summary of urban, aggressive, and taxi drivers' battery conditions at retirement under hot (H), cold (C), and reference (R) climates. Five retirement mileages (80,000, 120,000, 160,000, 200,000, and 240,000 km) were evaluated in this study. EV battery SOH (the color map), energy throughput (yellow bar plot), and in-vehicle operation service life (navy bar plots) at different mileages were extracted from our representative experimental study (Extended Data Table 3).* ***(b)*** *Summary of profile categories and the number of profiles collected across 16 countries, as identified in the literature and evaluated for second-life applications. Categories are defined based on power system applications, service types, or the type of information reported in the source studies: arbitrage (ARB), fast-charging stations (FCS), frequency regulation (FR), microgrids (MG), peak shaving (PS), volt–var control (VVC), and renewable energy storage (RES) (see Supplementary Table 16 for more details).*

(see Methods). The resulting RUL and energy throughput estimates were integrated with first-life EV usage data to quantify reuse value, with economic and resource efficiencies assessed using the levelized cost of storage (LCOS) and material cost reduction rate (MCRR), respectively (see Methods).

Our results suggest that reusing EV batteries can bring remarkable benefits. It improves the resource efficiency by up to 73.6% (Fig. 3a, quantified by MCRR) and extends battery overall lifetime by 5–7 years, based on an average EV lifetime of 200,000 km[5]. However, improper retirement and reuse may even reduce the original EV lifecycle values, resulting in negative MCRR (Fig. 3a, urban (H)). Therefore, we apply the following criteria to evaluate the reuse potential of EV batteries retired at different mileages and identify beneficial second-life scenarios: (1) retirement for reuse helps improve resource efficiency (resulting in a positive MCRR); (2) retirement for reuse before EOL can generate higher lifecycle value; and (3) EV batteries have at least 5 years of RUL in second-life applications[40].

Figure 3b (from left to right) presents the percentage of available second-life scenarios after sequentially applying criteria (1) to (3). Among all criteria, criterion (3) excludes the majority of second-life scenarios, indicating that the remaining lifetime of retired EV batteries is the primary constraint on reuse potential. Early retirement can help mitigate this limitation. For example, the batteries of aggressive, urban drivers can be reused in more applications when retired at lower mileage because of better health conditions, thereby increasing their RUL in second-life applications. However, early retirement should be avoided for other drivers whose batteries experience slower

degradation in EVs compared with second-life scenarios. This is because the shortened in-vehicle operation reduces the total life cycles of the batteries. For instance, taxi (C) batteries retired at 80,000 km have sufficient lifetime for most subsequent reuse scenarios, yet reusing them in only 13 % of the scenarios improves their overall lifecycle values (Fig. 3b center). In this case, the reuse potential is determined by both lifecycle values and the remaining lifetime of retired batteries (Fig. 3b center and right). Additionally, resource efficiency is rarely the constraint, given that reusing EV batteries generally provides greater lifecycle value than direct recycling due to higher energy throughput. Overall, an identical retirement strategy would not yield optimal results for heterogeneous EV batteries, underscoring the importance and urgency of retirement strategies tailored to diverse EV drivers to ensure reliable and valuable battery reuse.

Proactive trade-in strategy design

Trade-in strategies can guide EV owners to retire their batteries, offering financial benefits while respecting their preferences. We identify the optimal trade-in mileages and strategies for each type of driver, considering the following three priorities: (1) minimizing the LCOS during reuse (cost-driven); (2) maximizing the MCRR (resource-driven); and (3) striking the balance between (1) and (2) by providing Pareto fronts. Fig. 4a shows the distribution of optimal trade-in mileages for each type of driver (see Methods). Notably, different priorities lead to distinct trade-in strategies. The resource-driven strategy prefers an earlier trade-in at 80,000 km because EV batteries can have a longer overall lifetime, thereby achieving a higher MCRR (Fig. 4a). However, earlier trade-in is not always preferable, as we assume the cost of retired batteries is proportional to their remaining capacity. As a result, the cost-driven strategy suggests a more case-by-case trade-off in terms of trade-in mileage (Fig. 4a), because the LCOS depends on both the costs and the RUL of EV batteries (the denominator of LCOS) in each second-life application.

The proactive strategy that aligns with the triple bottom line[41] should balance between unit costs and resource savings while considering the warranty effect on EV owners' motivation. Fig. 4b summarizes the suggested trade-in mileage for each type of driver with the warranty period highlighted in yellow (8 years or 160,000 km, whichever comes first). Notably, our result suggests that most EV owners should trade in their batteries slightly before or after the warranty to achieve optimal lifecycle values. As evidenced by optimal retirement mileage at 80,000 km for urban (R, H) and aggressive (C) drivers, and 120,000 km for urban (C) and aggressive (H) drivers. A trade-in before warranty expiration is generally not recommended for taxi drivers, as their in-vehicle operation period typically lasts only 2–4 years. Also, early trade-in for reuse before 240,000 km is not recommended for aggressive (R) and taxi (H) batteries (Fig. 4b).

While the non-proactive strategy could be effective with subsidies, trade-in for reuse offers a proactive retirement pathway that naturally serves as a market mechanism that could benefit both OEMs and EV owners. EV owners are offered premium trade-in prices for retiring batteries at recommended mileages—typically 1–2 years earlier than the 160,000 km benchmark retirement practice. Trade-in reduces owners' expected out-of-pocket replacement costs and post-warranty failure risk. Crucially, our trade-in strategies centralize EV battery recollection from previous fragmented secondary markets and make the estimated 40–50% of retired batteries, which are deemed unreusable under current passive retirement practices, become viable for second-life applications, with at least five additional years of service (9.5 years on average, Supplementary Note 7).

Generalization in proactive strategy

We identify a simple indicator, the capacity-to-resistance change index (C2R), that links battery heterogeneity to optimal trade-in mileages (proof by a statistically significant linear relationship as shown in Fig. 4c, $p = 0.00187$). It provides a general rule for estimating the optimal trade-in mileages for real-world EV batteries. Beyond the representative drivers analyzed in this study, C2R can be calculated using BMS capacity and resistance recordings to inform real-time retirement mileages.

For batteries with different designs or chemistries, OEMs can still suggest trade-in mileages, use the PAL framework to establish the relationships between indicator values and optimal retirement mileages, or base it on prior knowledge of battery design. For example, the commercial EV battery analyzed in this study has an energy-type design and typically has a longer lifecycle when used for energy-oriented applications. Given that C2R reflects how degradation affects batteries' power and energy performance, a higher C2R suggests the battery is experiencing

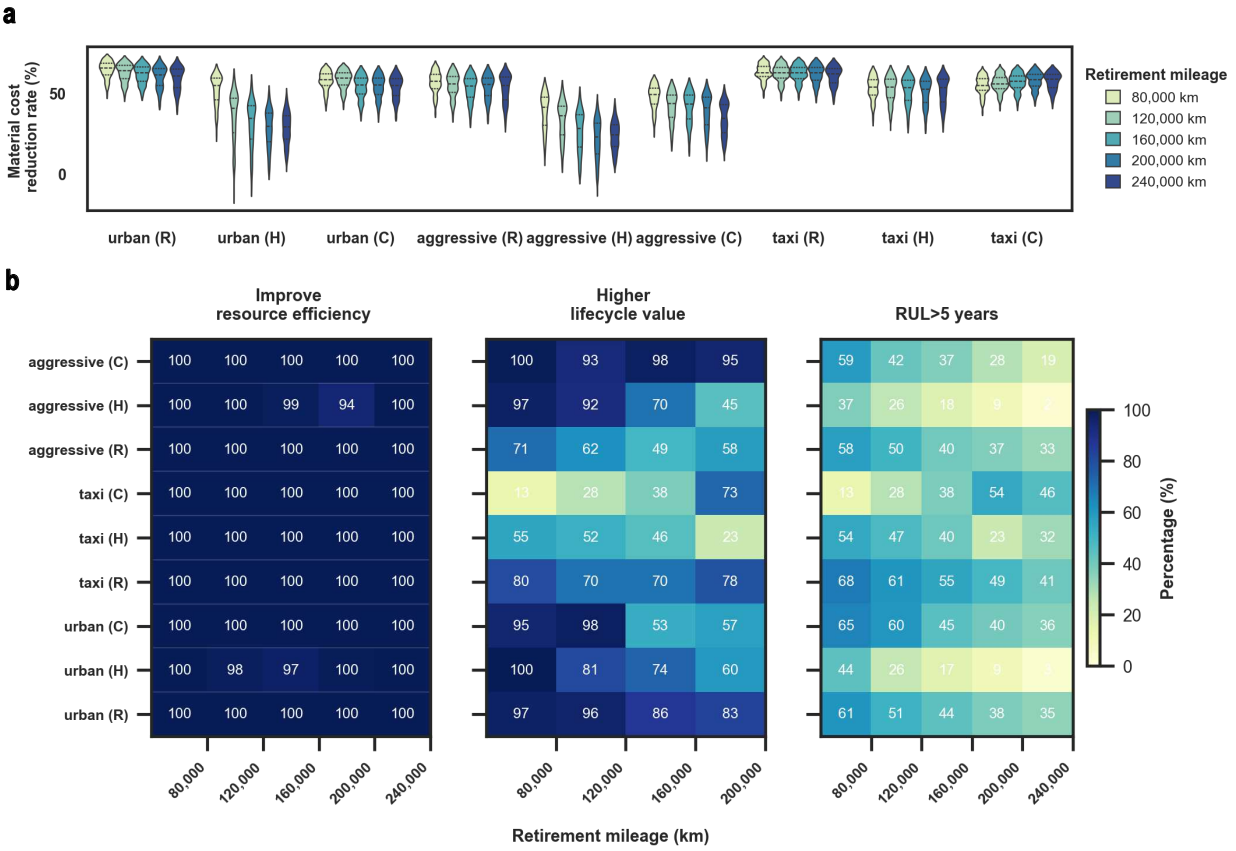


Fig. 3: *Impact of retirement mileage on reuse potential of EV batteries.* ***(a)*** *Statistical distribution of the lifecycle MCRR of EV batteries retired at different mileages and reused across 243 second-life scenarios.* ***(b)*** *Percentage of available second-life scenarios for EV batteries retired under different combinations of driving habits, climates, and retirement mileages. Subplots from left to right show the remaining percentages after the criteria are sequentially applied to screen out non-beneficial second-life scenarios.*

faster thermodynamic degradation, primarily reducing its energy capability. In contrast, a lower C2R indicates faster kinetic degradation, resulting in reduced power capability. Therefore, EV batteries with high C2R should continue to be used in their current application, such as in-vehicle operation. In contrast, the battery's power capability becomes the limiting factor, making it less suitable for vehicular use; such batteries should be retired earlier and reused for applications with lower power demands, for example, long-duration grid energy storage.

Discussion

Our findings challenge current passive retirement practices and suggest that a key bottleneck for EV battery reuse is the lack of effective retirement guidance. Under current practice, many retired EV batteries have limited reuse potential because of high lifetime uncertainty, reinforcing the misconception that EV battery reuse is generally not beneficial. More critically, this misconception can distort assessments of policies aimed at improving EV battery circularity and bias EOL management toward direct recycling. By contrast, accurately estimating how retirement practices affect EV battery reuse value can enable more targeted and effective policy interventions. We found that a minor change to current retirement practice can shift nearly half of EV batteries from being unreusable to reusable. Even under substantial uncertainty in reuse value, where second-life battery lifetime is intentionally underestimated, strategic retirement still benefits 30–45% of EV batteries (Supplementary Note 7). In practice, with strategic interventions, such as trade-in programs, OEMs could generate downstream revenue by reselling retired EV batteries for local energy storage applications, while EV owners could receive higher returns for retiring batteries at appropriate times.

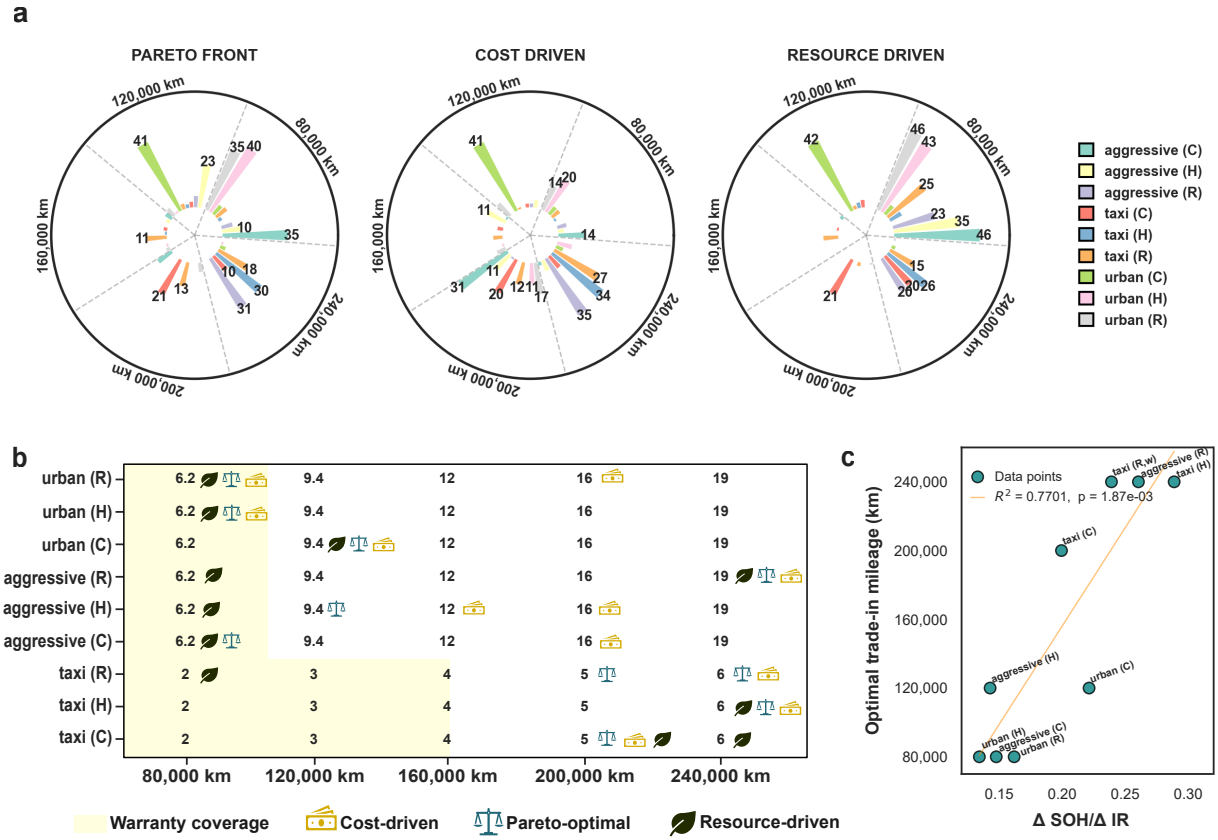


Fig. 4: *Optimal trade-in mileage and estimated RUL of EV batteries across second-life applications.* ***(a)*** *Number of viable second-life applications (out of 56) for each driver type under Pareto-front, cost-driven, and resource-driven strategies at trade-in mileages yielding maximum lifecycle value (summarized from Extended Data Fig. 3-5).* ***(b)*** *Recommended trade-in mileage for each driver type under Pareto-front (blue balance marker), cost-driven (yellow money icon), and resource-driven (green leaf icon) strategies. Numbers indicate the years required for each driver type to reach the corresponding mileage. The light yellow background indicates the warranty coverage of most EV batteries with 8 years or 160,000 km, whichever comes first. (c) Relationship between C2R and the optimal trade-in mileage.*

Given timely evaluation of the EV batteries' reuse value is critical for efficient EOL management, we present the first unified and scalable PAL framework for predictive lifecycle analysis of EV batteries across their first-life and second-life uses. It provides industrial stakeholders, such as battery OEMs, with accessible tools for identifying optimal lifecycle decision pathways. Another central finding is that the optimal retirement timing of EV batteries should be determined by their degradation behavior during in-vehicle use, rather than by applying a fixed threshold. Beyond applying the C2R indicator to suggest dynamic retirement timing, OEMs could use this indicator as a design factor for next-generation EV batteries to reduce their heterogeneity at retirement. For example, the battery module and pack designs can be tailored to different ranges, driving styles, and climate requirements and target similar C2R trajectories over time. Compared with existing solutions that rely on different chemistries to meet distinct design requirements, this approach could make batteries with similar remaining capacity more likely to have comparable reuse potential.

Several limitations remain, and future research directions are discussed in Supplementary Note 8. Overall, our work highlights the importance of strategic planning in preventing and addressing sustainability challenges.

Methods

Design validation data from OEM

In order to evaluate the cycle-life performance of commercial electric vehicle (EV) batteries, original equipment manufacturers (OEMs) often conduct comprehensive design validation tests to confirm the cycle-life of their batteries under various operating conditions. The design validation dataset used in this study was collected from Farasis Energy USA, which comprises cycle-life tests of 39 large-format lithium-ion pouch cells (76 Ah) with an

NMC811 cathode and a graphite anode. The dataset includes cycle-life tests under (1) real-world driving profiles, (2) calendar aging profiles, (3) standard constant-current-constant-voltage (CCCV) charging with constant-current (CC) discharging profiles, and (4) multi-stage constant current (MCC) charging with CC discharging profiles (Extended Data Table 1). These tests were performed under various ambient temperatures and discharge C rates. All battery cells were tested in environmental chambers with battery testers regulating current and voltage. In between cycles, the reference performance test (RPT) was conducted periodically at 25 °C to characterize the cell's remaining capacity and resistance (Supplementary Note 1).

Real-world driving cycle-life testing

To mimic the real-world EV driving conditions, the real-world driving testing protocols were constructed using representative battery discharging behaviors, charging behaviors, and seasonal climates summarized from aggregated EV user behavioral data provided by commercial partners (Supplementary Fig. 1). Driving behaviors were categorized into three groups (aggressive, urban, and taxi drivers (Supplementary Fig. 2a)) and the discharge current characteristics of each group were summarized in Supplementary Table 4. The taxi driver profile reflects consistent, low-variability load conditions typical of urban public transport, with frequent stops and moderate acceleration. The urban driver represents private city driving, characterized by variable loads due to traffic, braking, and acceleration. The aggressive driver simulates high-intensity operation with rapid acceleration and large current fluctuations. During cycle-life testing, battery cells were cycled under combinations of alternating discharge (Supplementary Fig. 2, orange curves), regenerative braking (Supplementary Fig. 2, purple curves) events with regenerative charging rates varying by temperature, and temperature-dependent charging. Level 1 and Level 2 charging (Supplementary Fig. 3) and multistage constant-current fast charging (Supplementary Fig. 2, green curves), where the charging rate was limited by the maximum allowable current for a given state-of-charge (SOC) and ambient temperature to prevent lithium plating, were assigned during the test (Supplementary Table 5). The ambient temperature during the cycle-life testing was controlled to represent three climate conditions—cold, reference, and hot—based on seasonal temperatures listed in Supplementary Table 3. The hot climate reflects persistently high-temperature regions such as Africa, the Middle East, and Southeast Asia. The reference climate represents areas with moderate seasonality, including central Europe, northern China, and the northeastern United States. The cold climate simulates subarctic and high-latitude regions such as Siberia, northern Canada, and Scandinavia. These temperature regimes were applied sequentially across spring, summer, autumn, and winter to reproduce the seasonal effects on battery aging and performance.

Other cycle-life testing

Calendar aging tests were performed at three SOC levels (30%, 80%, and 100%), and four temperatures (25 °C, 35 °C, 45 °C, and 60 °C) for 420 days (Extended Data Table 1). Cells were first charged to the target SOC and then stored in temperature-controlled environmental chambers. For cycle-life tests performed using a standard CCCV charging protocol and CC discharging, cells were charged at C/3 to an upper cutoff voltage of 4.2 V, followed by a constant-voltage hold until the current decreased to the cutoff threshold. Cells were then discharged at C/3 to a lower cutoff voltage of 2.75 V, corresponding to 100% depth of discharge (DOD). To investigate degradation under fast-charging conditions, MCC charging protocols were applied. In these tests, the charging current was varied across different SOC windows to prevent lithium plating during fast charging. The maximum charging rate ranged from 0.5C to 1.5C depending on the SOC window, while discharging was conducted at 1C. These experiments were performed over DOD windows ranging from 80% to 100% at ambient temperatures between 20 °C and 30 °C.

Extended experiments

In addition to the OEM datasets, 28 aged cells obtained from previous cycle-life tests with diverse historical cycling protocols were further tested under stationary energy storage operating conditions (with first-life operating conditions summarized in Supplementary Table 13). Specifically, six typical energy storage operation profiles were collected from the literature, representing grid services such as peak shaving, frequency regulation, and energy arbitrage across multiple countries (Extended Data Table 1). Each profile includes the current trajectory of a battery energy storage system over a typical 24-hour operating period. These aged cells were continuously cycled under these profiles to evaluate their remaining cycle-life. For comparison, six fresh cells were also tested under the same operating profiles as benchmark references. Prior to the cycle-life testings, diagnostic tests were conducted

on both fresh and aged cells to characterize their electrochemical characteristics (Supplementary Tables 1 and 2). Together with the cycle-life datasets provided by the OEM, these experimental datasets were used for physics-based model parameterization, scenario analysis of second-life applications, and the training and validation of the physics-guided machine learning models developed in this study.

Physics-augmented learning framework

We designed the physics-augmented learning (PAL) framework for EV battery predictive lifecycle analysis (Fig. 1d, Extended Data Fig. 7). This allows us to evaluate diverse lifecycle pathways from in-vehicle operation until various retirement timings to second-life applications. We first analyzed long-term aging under nine combinations of representative driving patterns and seasonal climates.

Then, we modeled battery dynamics and path-dependent degradation using the physics-based models for data augmentation. We used the design validation data to parameterize the pseudo-two-dimensional (P2D) electrochemical model and calibrate mechanistic aging sub-models to model their degradation, including solid-electrolyte-interphase (SEI) growth, lithium plating, and loss of active material on the cathode and anode. The modeling accuracy is validated using second-life experimental data from 28 aged batteries across six representative applications (Extended Data Table 1, Supplementary Table 13). Using this system, we generated high-throughput second-life battery datasets, worth 30,000 CPU core-hours of computation. It includes continuous degradation of aged batteries in up to 56 second-life applications (Fig. 2b, Supplementary Fig. 9, Supplementary Fig. 10), representing, to our knowledge, the most comprehensive power system operating profiles.

Lastly, we trained a physics-guided machine-learning model using both augmented and experimental datasets (Extended Data Table 1) to align aging physics from mechanistic sub-models with experimental data. Therefore, this model can reliably predict battery remaining useful life (RUL) in second-life applications that are not covered in the experimental study. Overall, we use 75 battery cell data for the PAL framework calibration and validation (Extended Data Fig. 2), and it allows us to perform a large-scale virtual exploration of 10,935 EV battery lifecycle scenarios (Extended Data Fig. 1).

Physics-based modeling

The physics-based models from open research software, PyBaMM[42], consist of (1) battery dynamic modeling and (2) battery degradation modeling. Specifically, battery dynamics were modeled using a pseudo-two-dimensional (P2D) model, namely the Doyle–Fuller–Newman (DFN) model, coupled with a lumped thermal model to capture its temperature-dependent characteristics[43]. These models were parameterized using cell design parameters provided by manufacturers (Supplementary Table 6) and material properties extracted from literature (Supplementary Tables 7 and 8), and all other parameters were fitted using diagnostic datasets (Supplementary Table 9). Fitting parameters were determined sequentially using open-circuit voltage data, as well as data collected from three CC discharge processes at different C rates and synthesized dynamic charging–discharging profiles. Model validation was performed under eight operating conditions, including seven power system operating profiles and one driving profile (Supplementary Note 3). To model battery long-term degradation behaviors, we integrated the parameterized P2D model with physics-based degradation sub-models in PyBaMM[42], including (i) solid electrolyte interface (SEI) growth, (ii) loss of active material (LAM) in both electrodes due to mechanical stress and particle cracking, and (iii) irreversible lithium plating. Following Safari et al.[44], the SEI growth was modeled as jointly governed by ethylene carbonate diffusion through the surface film and interfacial reaction kinetics, with the local current density described by a cathodic Tafel relation. For the anode, LAM is attributed to both stress-induced mechanisms (particle cracking and swelling) and reaction-driven processes associated with SEI growth. While for the cathode, LAM is only attributed to stress-induced mechanisms (particle swelling)[43,45]. Then, we parameterized the degradation sub-models by first fitting SEI growth model parameters using calendar aging data and then fitting LAM and lithium plating model parameters using cycling aging data (Supplementary Note 3)[46]. To ensure the model can accurately capture battery degradation behavior across diverse operating conditions, we parameterized these sub-models using cycling aging data collected under nine different conditions, including CCCV charging and CC discharge at C/3, six stationary energy storage operating profiles, and two CC discharge profiles with 1C MCC charging at 100% or 80% DOD (Extended Data Table 1). The optimal parameter set was identified by minimizing the mean absolute percentage error (MAPE) between experimental and simulated capacity degradation curves (Supplementary Fig. 7; Supplementary Tables 11 and 14, Supplementary Note 2).

To further validate the physics-based modeling fidelity in simulating and generating second-life battery long-term degradation, we evaluated the model performance on simulating the degradation of 28 aged batteries under six different profiles. We first parameterized the aged battery P2D models using diagnostic data detailed in Supplementary Table 2. Most of the P2D parameters remained the same as fresh batteries, and we mainly calibrated the subset that changes significantly over time, including active material volume fractions (cathode and anode), initial solid-phase lithium concentration, exchange current densities (cathode and anode), anode porosity, solid-phase diffusion coefficients of both electrodes, and the conductivity and diffusion coefficient of the electrolyte[43](Supplementary Fig. 5 illustrates examples of calibrated fits, with all calibration results summarized in Supplementary Table 10). Using calibrated P2D models of aged batteries as the starting point, we simulated their degradation trajectories and compared the simulated capacity degradation curve with the corresponding experimental measurements (Supplementary Fig. 8; Supplementary Table 13; Supplementary Note 3).

High-throughput data augmentation

Given limited experimental resources, we used the physics-based models to simulate the long-term degradation of aged batteries under diverse second-life operating scenarios. To expand the limited availability of open-source energy storage operating profiles, we conducted a comprehensive literature survey and compiled over 50 profiles spanning 16 countries. These profiles represent three stakeholder categories—customer, generation, and transmission—and cover major energy storage applications (Supplementary Tables 15 and 16). Each profile describes the operation of a battery energy storage system over a typical 24-hour period. To account for the influence of battery size on degradation and lifetime, battery capacity was discretized into eight representative configurations based on system constraints (e.g., maintaining SOC within [0, 1]), and the current profiles were scaled accordingly in the simulations (Supplementary Note 4).

To generate a high-throughput simulated dataset, we collected aged battery models obtained from first-life simulations. Each model was then subjected to continuous degradation simulations under second-life application profiles. Simulations were conducted for up to 2,500 equivalent full cycles (EFCs). Owing to the high computational cost of physics-based modeling, simulations were parallelized on high-performance computing clusters to accelerate data generation (Supplementary Note 4). In total, we generated over 600 long-term second-life battery degradation trajectories, capturing the cycle-life of aged batteries spanning diverse health conditions and second-life operating scenarios (Supplementary Fig. 10).

Physics-guided machine learning model

The physics-guided machine learning model employs a gradient boosting algorithm, CatBoost[47]. "Physics-guided" refers to a hybrid modeling approach that combines physics-based battery degradation modeling with data-driven modeling in a sequential manner[48]. Specifically, high-throughput simulation data generated by the physics-based models was used along with experimental data to train the CatBoost model. Model inputs comprised (i) battery health metrics, including capacity ($C_{\text{cell,rpt}}$), internal resistance (IR_{50}), and nonlinear combinations (e.g., $C_{\text{cell,rpt}} \times \text{IR}_{50}$, $C_{\text{cell,rpt}} \div \text{IR}_{50}$); (ii) degradation modes; and (iii) statistical features of operating profiles in the future where time-series statistics of current profiles were extracted, along with initial voltage and frequency-domain features (Supplementary Note 5). The output of the model was the RUL of the battery, defined as the number of EFCs to the knee point—the location on the degradation curve with the greatest perpendicular distance from the straight line connecting the start and end points—beyond which the battery has accelerated aging. The model was trained on 19,091 high-throughput simulated data points and 247 experimental data points. Each dataset was split into 80% for training and 20% for validation and then combined into training and validation datasets (Supplementary Note 5). Overall, the model resulted in a training error of 4.54% MAPE (mean absolute error: 38 EFC) and a validation error of 5.43% MAPE (mean absolute error: 45 EFC, Extended Data Fig. 2, Supplementary Note 2).

Systematic lifecycle analysis

To obtain EV battery health metrics at different retirement mileages, we first converted vehicle mileage into battery energy throughput. The energy throughput per cell W_{total} in kilowatt-hours (kWh) at given mileages D was calculated as:

$$W_{\text{total}} = \frac{2D}{n\eta} \tag{1}$$

where $n = 264$ denotes the total number of cells in the EV pack and η denotes the fuel efficiency, defined as the distance traveled per kWh of electrical energy consumed. Because both driving behavior and climate conditions influence the energy efficiency (Extended Data Table 3), we incorporated these factors when estimating fuel efficiency:

$$\eta = \frac{\eta_{\text{std}}}{\sigma} \tag{2}$$

where η_{std} and σ denote the empirical fuel efficiency and temperature coefficient, respectively. The values of η_{std} for urban, aggressive, and taxi driving behavior are 5.8, 4.4, and 5.1, respectively[39]. The values of σ for cold climate, reference climate, and hot climate are 1.3, 1.0, and 1.1, respectively[39]. And the EV battery service time (T_{total}) at a given mileage was calculated using $T_{\text{total}} = \frac{D}{d}$. The annual mileage d of urban drivers and aggressive drivers is assumed to be 12815 km[5,49], and that of taxi drivers is set to be 40233 km[50].

Using energy throughput at different mileages, battery health metrics were derived from experimental data and augmented with modeled calendar aging effects (Supplementary Note 1). The resulting health metrics, along with features of second-life operating profiles, were used as inputs for the physics-guided machine learning model to estimate battery RUL across various second-life scenarios. For full lifecycle evaluation, we combined the estimated second-life scenario information, including lifetime, energy throughput, and RUL, with the corresponding information extracted from real-world driving experimental data. Specifically, the remaining lifetime (days) of retired EV batteries was calculated by dividing the RUL in EFC by the daily EFC of the second-life profiles. The energy throughput (kWh) was then calculated by multiplying the remaining lifetime by the daily energy throughput.

To evaluate the reuse potential of EV batteries, the second-life RUL, lifecycle material cost reduction rate (MCRR), and marginal worth of early retirement were used as key criteria. Specifically, MCRR assesses the impact of battery reuse on reducing dependence on raw materials required to meet the rapidly growing energy storage demand, defined as:

$$MCRR = \frac{LCOM_{\text{ev}} - LCOM_{\text{ev+sl}}}{LCOM_{\text{ev}}} \tag{3}$$

where $LCOM$ denotes the simplified levelized cost of materials per unit of energy storage (Supplementary Note 6). A higher $MCRR$ indicates a greater reduction in raw material consumption per kWh of energy storage, thereby implying enhanced environmental benefits. The marginal worth of early retirement (M_{er}) is used to determine whether early retirement before 240,000 km is worthy. M_{er} describes the relationship between the gain in early retirement for reuse compared with the loss in EV operation due to early retirement and is defined as:

$$M_{\text{er}} = (THP_{\text{sl,D}} - THP_{\text{sl,240,000km}}) - (THP_{\text{ev,240,000km}} - THP_{\text{ev,D}}) \tag{4}$$

where $THP_{\text{sl,D}}$ is the second-life energy throughput of using EV batteries retired at mileage D and $THP_{\text{ev,D}}$ is the energy throughput of the EV batteries at mileage D. If M_{er} is greater than zero, the early retirement is worthy because it helps increase battery lifecycle values, and if its value is below zero, then continuing to use it in EVs leads to a higher lifecycle value than retirement for reuse. Together with lifetime requirements (RUL $\geq$ 5 years during second-life), the reuse potentials of retired EV batteries in second-life scenarios were evaluated.

To determine the optimal retirement mileage for each driver type under each second-life application, we first identified the optimal battery sizes and then determined the corresponding retirement mileages under different optimization objectives: (1) minimizing levelized cost of storage for a cost-driven solution (Supplementary Note 6); (2) maximizing MCRR for a resource-driven solution; and (3) identifying Pareto-optimal solutions considering both objectives (1) and (2). For objectives (1) and (2), the optimal solution was obtained by comparing the single-objective values across all scenarios and selecting the retirement mileage that yielded the best objective value. The third objective was formulated as a multi-objective optimization problem. We identified the Pareto front solutions that represent trade-offs between objectives (1) and (2), where improvement in one objective leads to deterioration

in the other[51]. To obtain a single balanced Pareto-optimal solution, we applied the Euclidean distance-to-utopia-point method, which selects the Pareto solution closest to the utopia point. The utopia point is defined by the minimum value of objective (1) and the maximum value of objective (2).

Retirement indicator

The capacity-to-resistance change index was calculated as the slope of resistance growth in percentage versus capacity loss in percentage (Extended Data Table 2) over the mileage range of 80,000 to 240,000 km. The resistance here was measured at 50% SOC under a 30-second 1C discharge current pulse.

Acknowledgments. This work is sponsored by Farasis Energy USA through its collaboration with the University of Michigan and the National University of Singapore. The authors thank Professor Johanna Mathieu from the University of Michigan for insightful discussions and constructive suggestions on the project and manuscript. The author would like to thank Yuanhao Cheng, Marcus Xavier Wen, and Xinyi Liu for their support in the application profile searching processes. The author would like to acknowledge the use of the high-performance computer from the National Supercomputing Centre of Singapore.

References

[1] Wang, C.-Y. *et al.* Fast charging of energy-dense lithium-ion batteries. *Nature* **611**, 485–490 (2022). URL https://www.nature.com/articles/s41586-022-05281-0.

[2] Yang, C. *et al.* Addressing the safety of next-generation batteries. *Nature* **645**, 603–613 (2025). URL https://www.nature.com/articles/s41586-025-09358-4.

[3] Trends in electric cars – global EV outlook 2026 – analysis. URL https://www.iea.org/reports/global-ev-outlook-2026/trends-in-electric-cars.

[4] Tian, X. *et al.* Sustainable battery recycling through spatial and technological alignment 1–15. URL https://www.nature.com/articles/s41893-026-01851-6.

[5] Nguyen-Tien, V., Zhang, C., Strobl, E. & Elliott, R. J. R. The closing longevity gap between battery electric vehicles and internal combustion vehicles in Great Britain. *Nature Energy* **10**, 354–364 (2025). URL https://www.nature.com/articles/s41560-024-01698-1.

[6] Busch, P., Chen, Y., Ogbonna, P. & Kendall, A. Effects of demand and recycling on the when and where of lithium extraction. *Nature Sustainability* **8**, 773–783 (2025). URL https://www.nature.com/articles/s41893-025-01561-5.

[7] Wu, Y. *et al.* Impact of circular economy on the long-term allocation structure of primary and secondary lithium **5**, 503. URL https://www.nature.com/articles/s43247-024-01667-2.

[8] Lakeman, S. Lithium triangle supply chains **10**, 6–7. URL https://www.nature.com/articles/s41560-024-01673-w.

[9] Zhang, B. *et al.* Lithium-ion battery recycling relieves the threat to material scarcity amid china's electric vehicle ambitions **16**, 6661. URL https://www.nature.com/articles/s41467-025-61481-y.

[10] Zeng, A. *et al.* Battery technology and recycling alone will not save the electric mobility transition from future cobalt shortages **13**, 1341. URL https://www.nature.com/articles/s41467-022-29022-z.

[11] Wu, Y. *et al.* A circular economy approach for the global lithium-ion battery supply chain (2025). URL https://www.researchsquare.com/article/rs-5995588/v1.

[12] Aguilar Lopez, F., Lauinger, D., Vuille, F. & Müller, D. B. On the potential of vehicle-to-grid and second-life batteries to provide energy and material security **15**, 4179. URL https://www.nature.com/articles/s41467-024-48554-0.

[13] Zhu, L. *et al.* Reusing vehicle batteries can power rural China while contributing to multiple SDGs. *Cell Reports Sustainability* **1**, 100060 (2024). URL https://linkinghub.elsevier.com/retrieve/pii/S2949790624000727.

[14] Nurdiawati, A. & Agrawal, T. K. Creating a circular EV battery value chain: End-of-life strategies and future perspective. *Resources, Conservation and Recycling* **185**, 106484 (2022). URL https://linkinghub.elsevier.com/retrieve/pii/S0921344922003275.

[15] Ma, R. *et al.* Pathway decisions for reuse and recycling of retired lithium-ion batteries considering economic and environmental functions. *Nature Communications* **15**, 7641 (2024). URL https://www.nature.com/articles/s41467-024-52030-0.

[16] Castelvecchi, D. Electric cars and batteries: how will the world produce enough? *Nature* **596**, 336–339 (2021). URL https://www.nature.com/articles/d41586-021-02222-1.

[17] Humanity needs to diversify its lithium sources. *Nature* **637**, 1021–1022 (2025). URL https://www.nature.com/articles/d41586-025-00213-0.

[18] Chun, H. Y. & Park, T. J. How car and battery companies can work around US trade tariffs and rules. *Nature* **637**, 31–33 (2025). URL https://www.nature.com/articles/d41586-024-04168-6.

[19] Lithium-ion batteries need to be greener and more ethical. *Nature* **595**, 7–7 (2021). URL https://www.nature.com/articles/d41586-021-01735-z.

[20] Woodley, L., See, C. Y. & Nunes, A. Battery prices are falling, so why are electric cars still so expensive? *Nature* **644**, 608–610 (2025). URL https://www.nature.com/articles/d41586-025-02619-2.

[21] Qin, Y. *et al.* Lithium ion batteries participating in frequency regulation for power grid under the thermo-electric coupling degradation mechanisms **19**, 100290. URL https://www.sciencedirect.com/science/article/pii/S2590116823000656.

[22] Ohrelius, M., Lindbergh, G. & Lindström, R. W. Polarization effects and aging characterization of lithium-ion batteries for second life applications **655**, 237931. URL https://www.sciencedirect.com/science/article/pii/S0378775325017677.

[23] Gu, X. *et al.* Challenges and opportunities for second-life batteries: Key technologies and economy. *Renewable and Sustainable Energy Reviews* **192**, 114191 (2024). URL https://linkinghub.elsevier.com/retrieve/pii/S1364032123010493.

[24] Sinha, A., Wu, J., Sheraz, M. & Qin, Q. China needs to deal with discarded electric-vehicle batteries. *Nature* **641**, 594–594 (2025). URL https://www.nature.com/articles/d41586-025-01508-y.

[25] Rahwan, I., Shariff, A. & Bonnefon, J.-F. The science fiction science method. *Nature* **644**, 51–58 (2025). URL https://www.nature.com/articles/s41586-025-09194-6.

[26] Zhu, B. & Wei, C. Strategic interactions for carbon emissions in Chinese cities are influenced by mayors. *Nature Cities* **1**, 370–377 (2024). URL https://www.nature.com/articles/s44284-024-00059-z.

[27] Zheng, D. *et al.* Strategies for climate-resilient global wind and solar power systems. *Nature* **643**, 1263–1270 (2025). URL https://www.nature.com/articles/s41586-025-09266-7.

[28] Andrews, L. & Grantham, T. E. Strategic stream gauging network design for sustainable water management. *Nature Sustainability* **7**, 714–723 (2024). URL https://www.nature.com/articles/s41893-024-01357-z.

[29] Siqueira-Gay, J., Metzger, J. P., Sánchez, L. E. & Sonter, L. J. Strategic planning to mitigate mining impacts on protected areas in the Brazilian Amazon. *Nature Sustainability* **5**, 853–860 (2022). URL https://www.nature.com/articles/s41893-022-00921-9.

[30] Williams, D. R. *et al.* Proactive conservation to prevent habitat losses to agricultural expansion. *Nature Sustainability* **4**, 314–322 (2021). URL https://www.nature.com/articles/s41893-020-00656-5.

[31] Xu, B., Liu, Z., Yan, S., Schmitt, R. J. P. & He, X. Strategizing renewable energy transitions to preserve sediment transport integrity. *Nature Sustainability* 1–14 (2025). URL https://www.nature.com/articles/s41893-025-01626-5.

[32] Lazarus, J. V. *et al.* A multinational Delphi consensus to end the COVID-19 public health threat. *Nature* **611**, 332–345 (2022). URL https://www.nature.com/articles/s41586-022-05398-2.

[33] Ward, L. *et al.* Principles of the Battery Data Genome. *Joule* **6**, 2253–2271 (2022). URL https://www.sciencedirect.com/science/article/pii/S2542435122004093.

[34] Geslin, A. *et al.* Dynamic cycling enhances battery lifetime. *Nature Energy* **10**, 172–180 (2025). URL https://www.nature.com/articles/s41560-024-01675-8.

[35] Attia, P. M. *et al.* Closed-loop optimization of fast-charging protocols for batteries with machine learning. *Nature* **578**, 397–402 (2020). URL https://doi.org/10.1038/s41586-020-1994-5.

[36] Li, K., Wang, J., Song, Y. & Wang, Y. Machine learning-guided discovery of ionic polymer electrolytes for lithium metal batteries **14**, 2789. URL https://www.nature.com/articles/s41467-023-38493-7.

[37] Chen, B.-R. *et al.* Battery aging mode identification across NMC compositions and designs using machine learning. *Joule* **6**, 2776–2793 (2022). URL https://linkinghub.elsevier.com/retrieve/pii/S2542435122005256.

[38] Dufek, E. J., Tanim, T. R., Chen, B.-R. & Sangwook Kim. Battery calendar aging and machine learning. *Joule* **6**, 1363–1367 (2022). URL https://linkinghub.elsevier.com/retrieve/pii/S2542435122002549.

[39] Lee, G., Song, J., Lim, Y. & Park, S. Energy consumption evaluation of passenger electric vehicle based on ambient temperature under Real-World driving conditions. *Energy Conversion and Management* **306**, 118289 (2024). URL https://linkinghub.elsevier.com/retrieve/pii/S0196890424002309.

[40] Smith, K. A. Battery Second Use Analysis and Demonstration: Cooperative Research and Development Final Report, CRADA Number CRD-13 -537. Tech. Rep. NREL/TP–5400-72557, 1476983 (2018). URL http://www.osti.gov/servlets/purl/1476983/.

[41] on, K. M. The triple bottom line: What it is & why it's important. URL https://online.hbs.edu/blog/post/what-is-the-triple-bottom-line.

[42] Sulzer, V., Marquis, S. G., Timms, R., Robinson, M. & Chapman, S. J. Python battery mathematical modelling (PyBaMM) **9**. URL https://openresearchsoftware.metajnl.com/articles/10.5334/jors.309.

[43] O'Kane, S. E. J. *et al.* Lithium-ion battery degradation: how to model it. *Physical Chemistry Chemical Physics* **24**, 7909–7922 (2022). URL http://dx.doi.org/10.1039/D2CP00417H.

[44] Safari, M. & Delacourt, C. Aging of a Commercial Graphite/LiFePO4 Cell. *Journal of The Electrochemical Society* **158**, A1123 (2011). URL https://iopscience.iop.org/article/10.1149/1.3614529.

[45] Edge, J. S. *et al.* Lithium ion battery degradation: what you need to know. *Physical Chemistry Chemical Physics* **23**, 8200–8221 (2021). URL http://xlink.rsc.org/?DOI=D1CP00359C.

[46] Pannala, S., Movahedi, H., Garrick, T. R., Stefanopoulou, A. G. & Siegel, J. B. Consistently tuned battery lifetime predictive model of capacity loss, resistance increase, and irreversible thickness growth **171**, 010532. URL https://iopscience.iop.org/article/10.1149/1945-7111/ad1294.

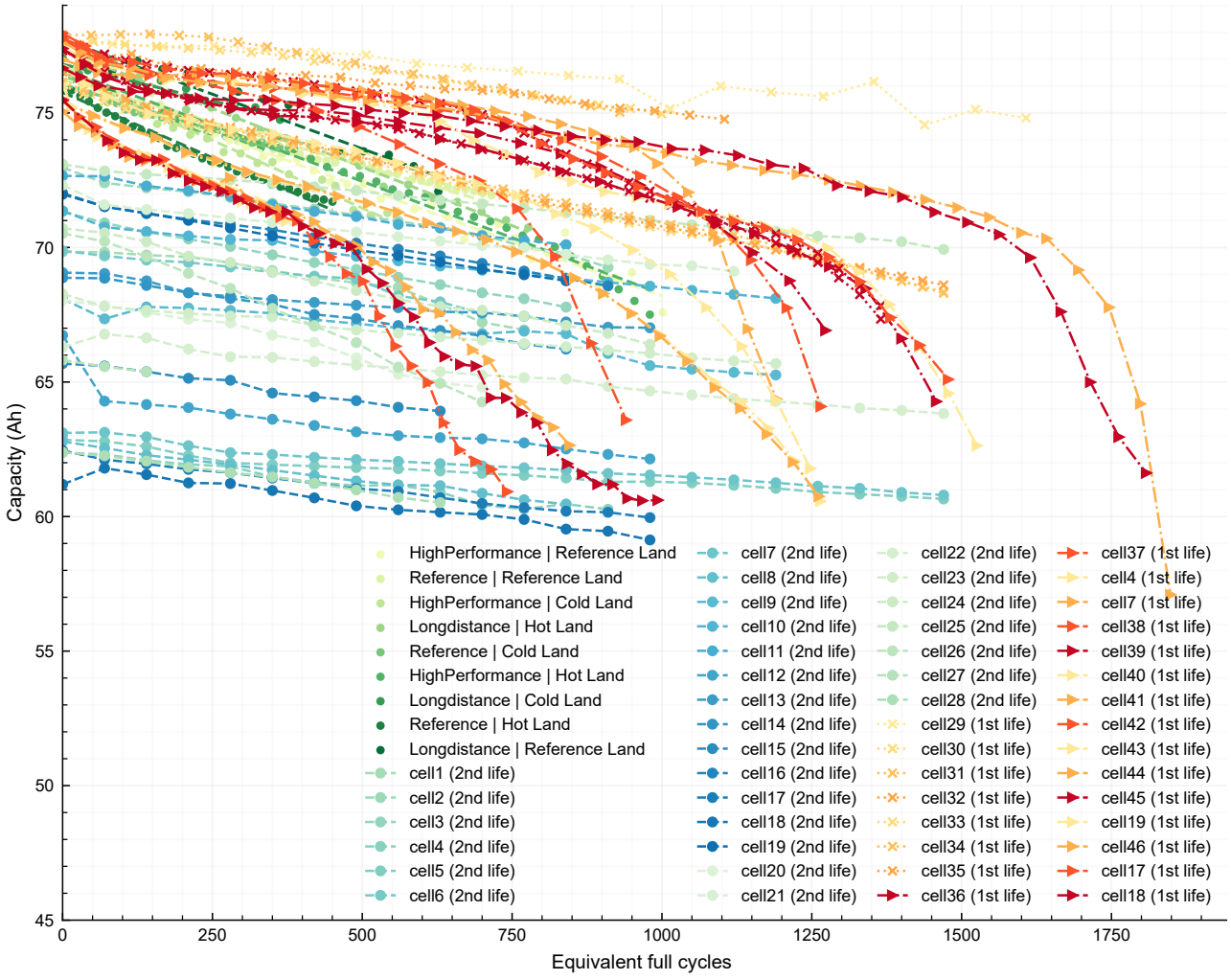
[47] Prokhorenkova, L., Gusev, G., Vorobev, A., Dorogush, A. V. & Gulin, A. CatBoost: unbiased boosting with categorical features (2019). URL http://arxiv.org/abs/1706.09516.

[48] Karniadakis, G. E. *et al.* Physics-informed machine learning. *Nature Reviews Physics* **3**, 422–440 (2021). URL https://www.nature.com/articles/s42254-021-00314-5.

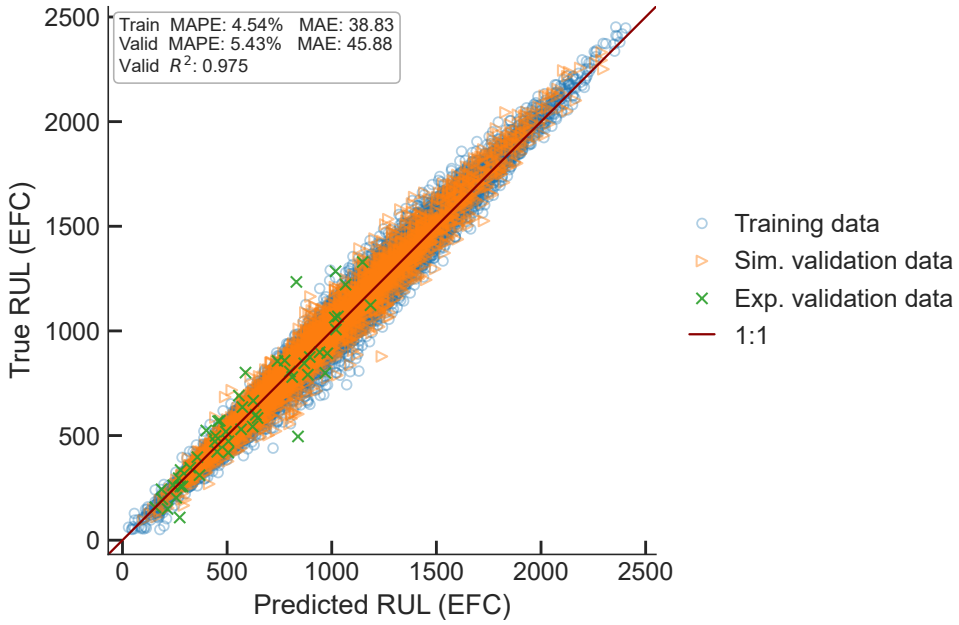
[49] Zhao, L., Ottinger, E. R., Yip, A. H. C. & Helveston, J. P. Quantifying electric vehicle mileage in the United States. *Joule* **7**, 2537–2551 (2023). URL https://linkinghub.elsevier.com/retrieve/pii/S254243512300404X.

[50] Richardson, P. What's the annual average mileage for a taxi driver and how does it vary from region to region? (2024). URL https://www.taxi-point.co.uk/post/what-s-the-annual-average-mileage-for-a-taxi-driver-and-how-does-it-vary-from-region-to-region.

[51] Alfaris, D. A. Multiobjective Optimization (II) .



Extended Data Fig. 1 | *Capacity fade versus equivalent full cycles for fresh and aged batteries. Scatter points show cell aging under EV driving profiles, with legend entries denoting driving behavior and temperature. Open circles with dashed lines represent aged cell degradation under continuous stationary energy storage use, cross marker with dotted lines denote fresh cells aged under stationary profiles, and triangular marker with dash-dot lines indicate fresh cells aged under constant-current, constant-voltage cycling.*



Extended Data Fig. 2 | *Predicted versus true cycle-life values for training and validation datasets. Training data (open circles) show close alignment with the 1:1 reference line (dark red), while validation data are separated into simulated cells (open triangles) and experimental validation cells (cross markers). Performance metrics are summarized (MAPE, MEA), highlighting the model's ability to predict the RUL of aged batteries across diverse second-life profiles.*

Extended Data Table 1 — *Overview of cycle-life experimental data.*

Cell types	Cycling profile	Temperature	Description	Purpose	Number
First-life	Real-world driving	Varied	See Method	Life cycle analysis & Catboost training	13
First-life	Calendar aging	25-60 ℃	Rest at 30%, 80%, 100% state of charge for 420 days	Calibrate physics-based SEI growth model & semi-empirical SEI growth model	8
First-life	CCCV	25 ℃	Constant current constant voltage charging and discharging at C/3, 100% DOD	Calibrate aging model (particle cracking, lithium plating) & Catboost training	5
First-life	MCC	20 ℃-30 ℃	Max C rate 0.5-1.5 C, 80-100% DOD, MCC charging process to the defined maximum C rate with 1 C constant current discharge	Calibrate aging model (particle cracking, lithium plating) & Catboost training	13
First-life	Profile 1	25 ℃	UK ARB, case 74	Calibrate the DFN & aging model	1
First-life	Profile 2	25 ℃	Standard FR protocol of US. Standards	Calibrate the DFN	1
First-life	Profile 3	25 ℃	- PS, case 79	Calibrate the DFN & aging model	1
First-life	Profile 4	25 ℃	China ARB, case 73	Calibrate the DFN & aging model	1
First-life	Profile 5	25 ℃	California PS, case 37	Calibrate the DFN & aging model	1
First-life	Profile 6	25 ℃	Michigan PS, case 50	Calibrate the DFN & aging model	1
First-life	Profile 7	25 ℃	Switzerland FR, case 30	Calibrate the DFN & aging model	1
Second-life	Profile 1	25 ℃	UK ARB, case 74	Validate aging model	5
Second-life	Profile 3	25 ℃	- PS, case 79	Validate aging model & Catboost training	5
Second-life	Profile 4	25 ℃	China ARB, case 73	Validate aging model	6
Second-life	Profile 5	25 ℃	California PS, case 37	Validate aging model	5
Second-life	Profile 6	25 ℃	Michigan PS, case 50	Validate aging model	5
Second-life	Profile 7	25 ℃	Switzerland FR, case 30	Validate aging model	4

Extended Data Table 2 *— EV battery health across driving behaviors, road conditions, and mileages. For each EV operating condition, defined by a combination of driving behavior and temperature, five trade-in scenarios are constructed. The EOL, SOH and internal resistance at different mileages were derived from experimental cycling data, with the effects of calendar aging incorporated using the calibrated semi-empirical model (Supplementary Fig.6).*

	Condition	Mileage	Throughput (kWh)	SOH (cycling)	IR (cycling)	Δ SOH (calendar,%)	Δ IR (calendar,%)	EOL SOH	EOL IR
0	urban (R)	80000 km	104.49	0.97	0.02	4.6	5.84	0.92	0.08
1	urban (H)	80000 km	114.94	0.96	0.07	8.5	31.19	0.88	0.38
2	urban (C)	80000 km	135.84	0.97	0.01	2.97	1.5	0.94	0.02
3	aggressive (R)	80000 km	125.39	0.97	0.02	4.5	5.5	0.93	0.08
4	aggressive (H)	80000 km	137.93	0.97	0.05	8.6	30.3	0.88	0.36
5	aggressive (C)	80000 km	163.01	0.95	0.07	3	1.5	0.92	0.08
6	taxi (R)	80000 km	118.84	0.99	0	2.36	1.58	0.97	0.02
7	taxi (H)	80000 km	130.72	0.97	0.1	4.56	9.24	0.92	0.19
8	taxi (C)	80000 km	154.49	0.98	0.03	1.09	0.2	0.97	0.03
9	urban (R)	120000 km	156.74	0.96	0.09	5.89	8.9	0.9	0.17
10	urban (H)	120000 km	172.41	0.95	0.11	10.66	46.84	0.85	0.58
11	urban (C)	120000 km	203.76	0.96	0.02	3.66	2.28	0.92	0.05
12	aggressive (R)	120000 km	188.09	0.96	0.04	5.9	8.2	0.9	0.12
13	aggressive (H)	120000 km	206.9	0.95	0.09	10.67	47.1	0.85	0.56
14	aggressive (C)	120000 km	244.51	0.93	0.17	3.7	2.3	0.9	0.19
15	taxi (R)	120000 km	178.25	0.98	0.04	2.86	2.35	0.95	0.06
16	taxi (H)	120000 km	196.08	0.96	0.12	5.64	11.46	0.9	0.24
17	taxi (C)	120000 km	231.73	0.97	0.08	1.43	0.34	0.95	0.08
18	urban (R)	160000 km	208.99	0.96	0.15	6.8	11.69	0.89	0.26
19	urban (H)	160000 km	229.89	0.94	0.15	12.05	63.76	0.82	0.78
20	urban (C)	160000 km	271.68	0.95	0.06	4.24	3.05	0.91	0.09
21	aggressive (R)	160000 km	250.78	0.95	0.08	6.7	12.3	0.88	0.2
22	aggressive (H)	160000 km	275.86	0.94	0.13	12.5	62.9	0.82	0.76
23	aggressive (C)	160000 km	326.02	0.91	0.3	4.2	3.12	0.87	0.33
24	taxi (R)	160000 km	237.67	0.96	0.11	3.25	2.99	0.93	0.14
25	taxi (H)	160000 km	261.44	0.94	0.15	6.22	16.83	0.88	0.32
26	taxi (C)	160000 km	308.97	0.95	0.15	1.71	0.49	0.94	0.15

Continued on next page

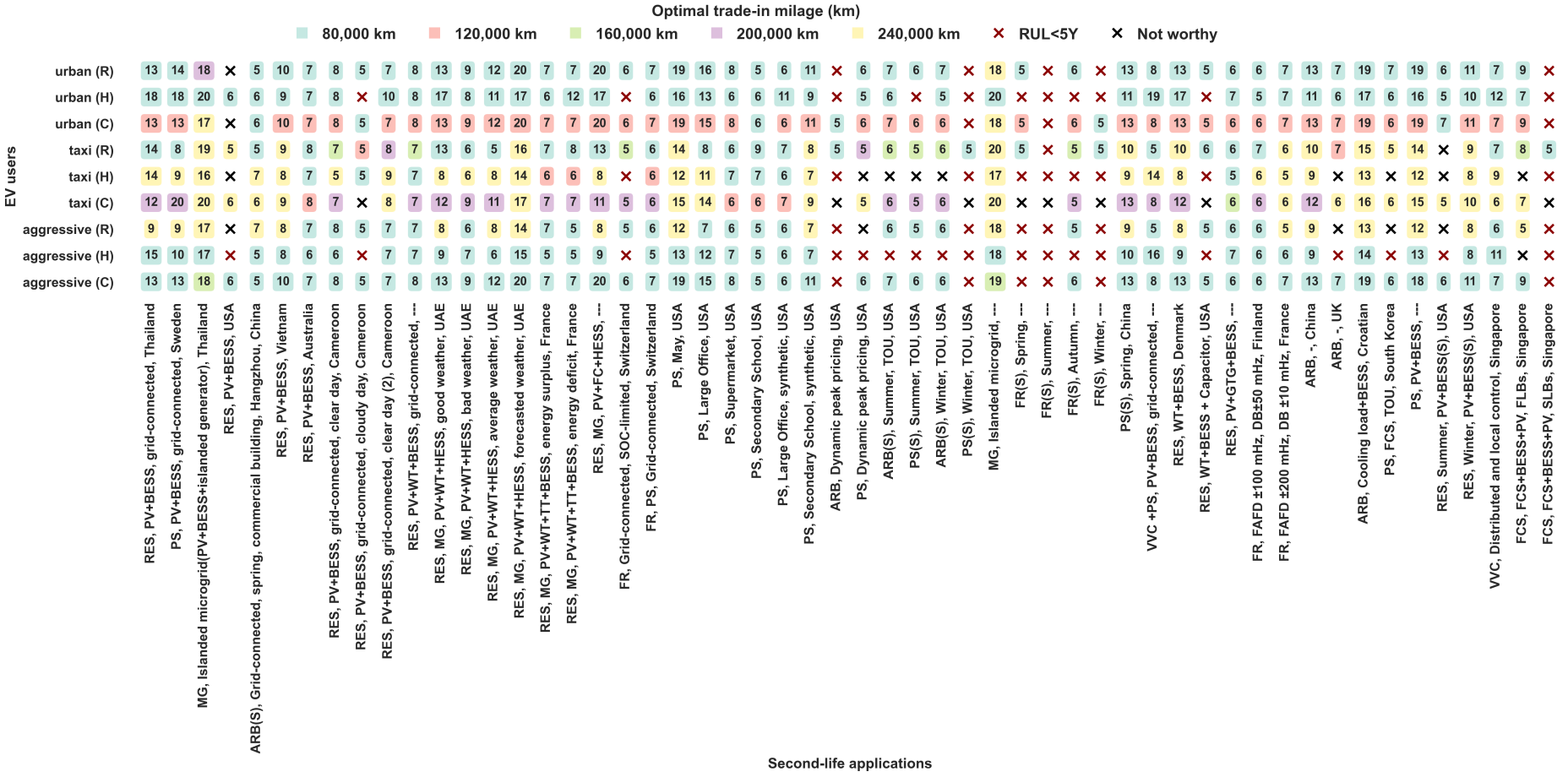
	Condition	Mileage	Throughput (kWh)	SOH (cycling)	IR (cycling)	Δ SOH (calendar,%)	Δ IR (calendar,%)	EOL SOH	EOL IR
27	urban (R)	200000 km	261.23	0.95	0.2	7.48	15.32	0.87	0.35
28	urban (H)	200000 km	287.36	0.93	0.18	13.89	83.62	0.79	1.01
29	urban (C)	200000 km	339.6	0.94	0.12	4.75	3.83	0.89	0.16
30	aggressive (R)	200000 km	313.48	0.94	0.13	7.4	15.3	0.87	0.28
31	aggressive (H)	200000 km	344.83	0.93	0.17	13.3	83.9	0.79	1.01
32	aggressive (C)	200000 km	407.52	0.9	0.47	4.8	3.9	0.85	0.51
33	taxi (R)	200000 km	297.09	0.95	0.18	3.66	3.67	0.91	0.21
34	taxi (H)	200000 km	326.8	0.93	0.18	6.88	20.52	0.86	0.38
35	taxi (C)	200000 km	386.22	0.94	0.22	1.95	0.64	0.92	0.23
36	urban (R)	240000 km	313.48	0.94	0.26	7.53	17.56	0.87	0.43
37	urban (H)	240000 km	344.83	0.92	0.21	15.34	97.18	0.77	1.18
38	urban (C)	240000 km	407.52	0.93	0.22	5.22	4.61	0.88	0.26
39	aggressive (R)	240000 km	376.18	0.93	0.19	8.3	19.04	0.85	0.38
40	aggressive (H)	240000 km	413.79	0.91	0.21	15.8	96.6	0.76	1.18
41	aggressive (C)	240000 km	489.03	0.88	0.68	5.28	4.7	0.82	0.73
42	taxi (R)	240000 km	356.51	0.93	0.26	3.88	4.42	0.9	0.31
43	taxi (H)	240000 km	392.16	0.92	0.21	7.4	24.74	0.85	0.46
44	taxi (C)	240000 km	463.46	0.93	0.31	2.16	0.78	0.91	0.32

Extended Data Table 3 *— Real-world annual mileage and fuel efficiency of each type of EV driver at hot climate, cold climate, and reference climate.*

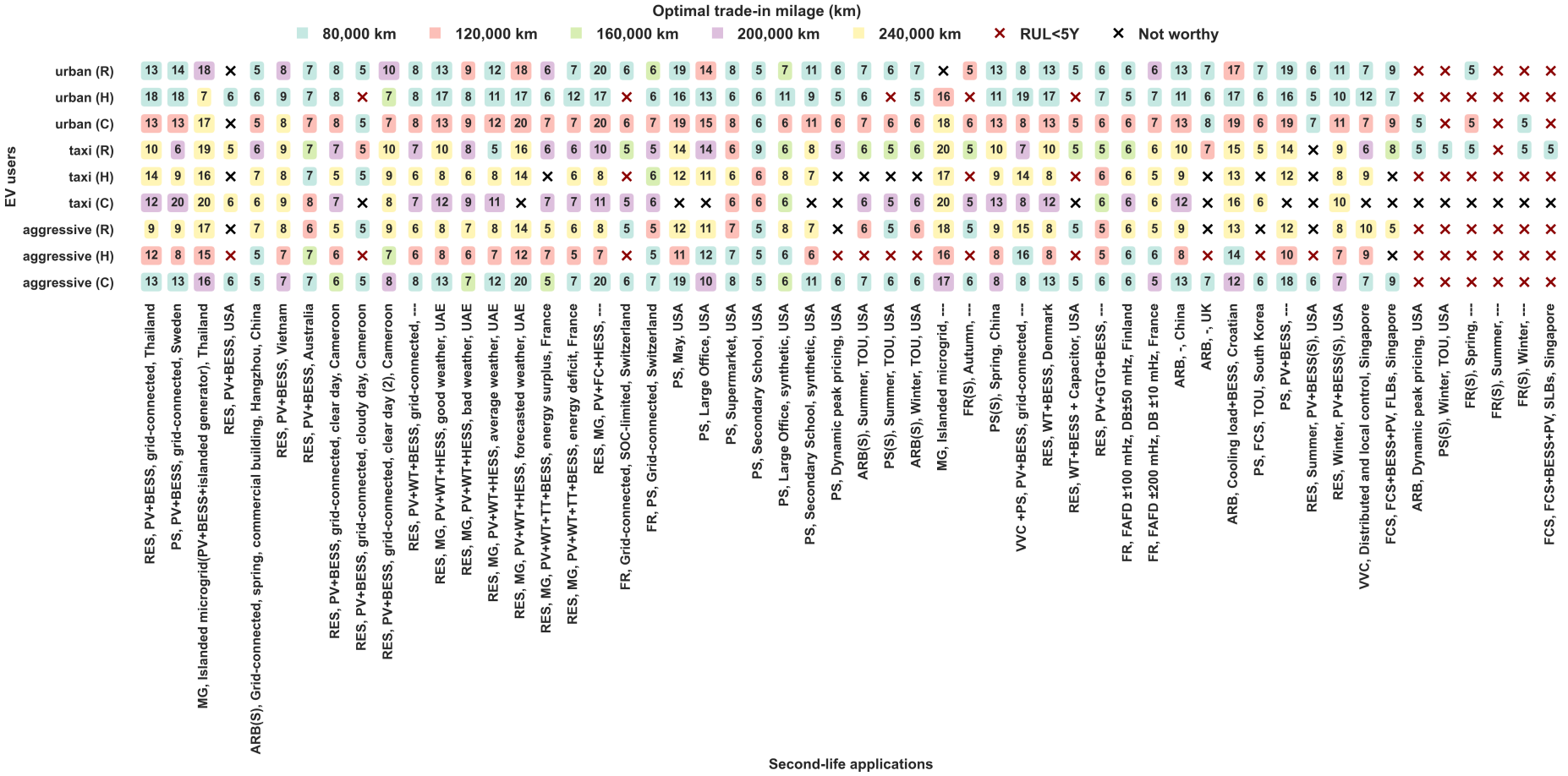
Category	Mileage per year d (km)	Fuel efficiency η (km/kWh)
urban (R)	12815.17	5.80
urban (H)	12815.17	5.27
urban (C)	12815.17	4.46
taxi (R)	40233.50	5.10
taxi (H)	40233.50	4.64
taxi (C)	40233.50	3.92
aggressive (R)	12815.17	4.83
aggressive (H)	12815.17	4.39
aggressive (C)	12815.17	3.72



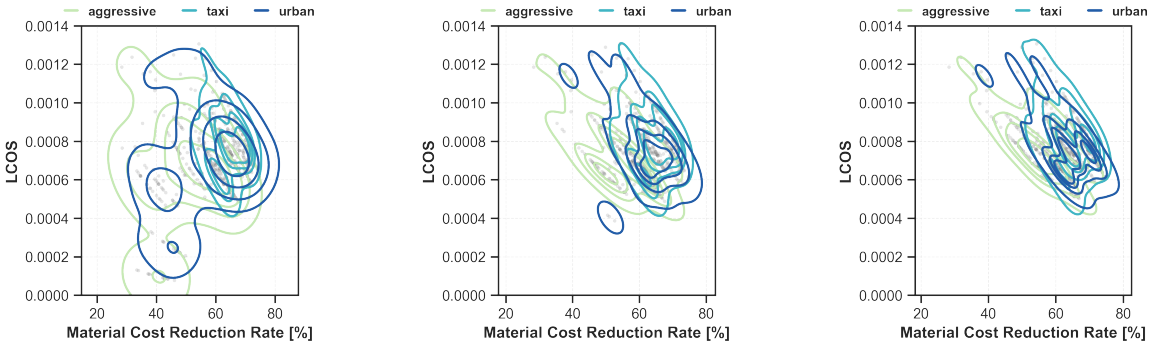
Extended Data Fig. 3 | *Recommended trade-in mileage (filed in color) and corresponding second-life RUL (numbers within rectangular shape) for each driver–application pair for the cost-driven solution. Red and black crosses mark infeasible applications, excluded due to insufficient lifetime (RUL $\leq$ 5 years) or limited value (where early retirement does not increase lifetime throughput). Second-life applications that are infeasible for all drivers are not shown in the figure.*



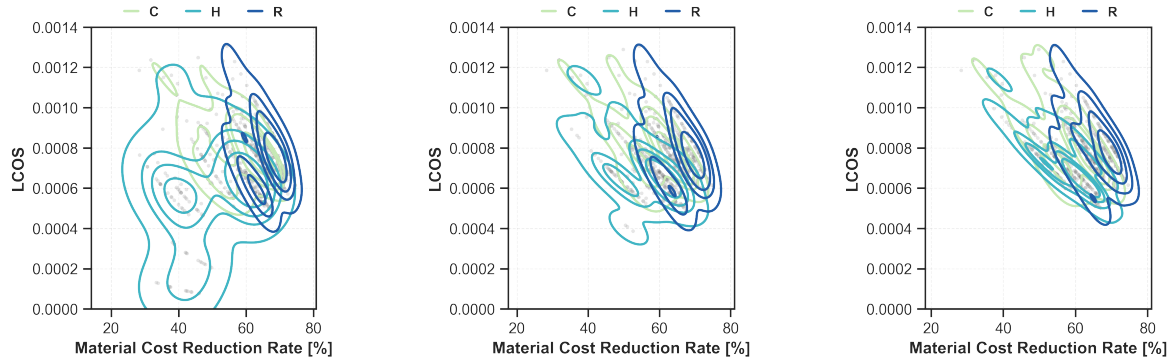
Extended Data Fig. 4 | *Recommended trade-in mileage (filed in color) and corresponding second-life RUL (numbers within rectangular shape) for each driver–application pair for the resource-driven solution. Red and black crosses mark infeasible applications, excluded due to insufficient lifetime (RUL $\leq$ 5 years) or limited value (where early retirement does not increase lifetime throughput). Second-life applications that are infeasible for all drivers are not shown in the figure.*



Extended Data Fig. 5 | *Recommended trade-in mileage (filed in color) and corresponding second-life RUL (numbers within rectangular shape) for each driver–application pair for the Pareto front solution. Red and black crosses mark infeasible applications, excluded due to insufficient lifetime (RUL $\leq$ 5 years) or limited value (where early retirement does not increase lifetime throughput). Second-life applications that are infeasible for all drivers are not shown in the figure.*

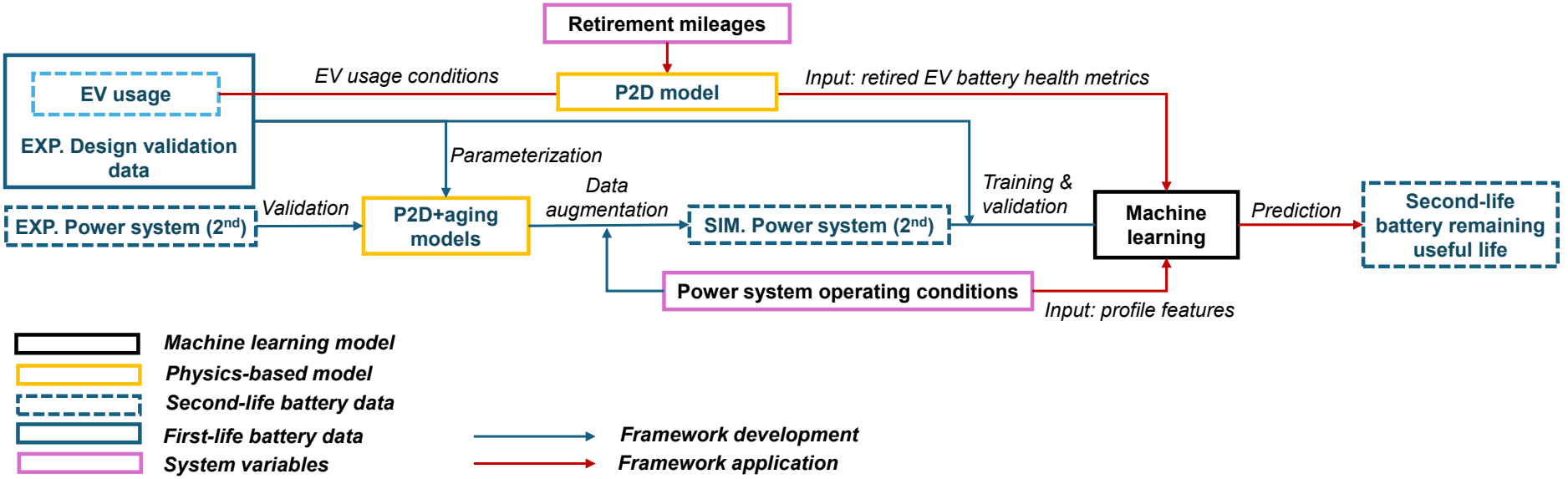


a *Cost-driven solution* ***b*** *Pareto front solution* ***c*** *Resource-driven solution*



d *Cost-driven solution* ***e*** *Pareto front solution* ***f*** *Resource-driven solution*

Extended Data Fig. 6 | *The contour plot shows the effects of driver behaviors (a-c) and climates (d-f) on resulting material cost reduction per kWh and LCOS of cost-driven, Pareto front, and resource-driven solutions.*



Extended Data Fig. 7 | *Flow chart of the PAL framework. Arrow colors indicate two workflows: the framework development process (including parameterization, validation, and data generation) and its application to generate the results reported in this study.*